Supplementary Information

For

Hierarchical structures of surface-accessible plasmonic based on gold and silver nanoparticles for SERS detection

Nhu-Bao Trinh[1,2], Thu Anh Nguyen[1,2], Son-Hai Lam Truong[1,2], Khuong Quoc Vo[1,2,*]

[1] Faculty of Chemistry, Ho Chi Minh City University of Science, Vietnam National University, Ho Chi Minh City, 227 Nguyen Van Cu Street, Ward 4, District 5, Ho Chi Minh City 70000, Vietnam.

[2] Vietnam National University, Ho Chi Minh City, Vietnam.

* Corresponding author

Email: vqkhuong@hcmus.edu.vn

Nanoarray

Nanoarray was a structured arrangement of nanoparticles organized in a periodic or predefined pattern on a surface. [1]. In this study, the choice of nanoarray structure to investigate was important because it offers distinct advantages over colloidosome and Pickering emulsion structures. Nanoarrays are highly ordered structures in which nanoparticles are systematically arranged on a surface, creating a dense network of “hot spots”. [2] This is distinct from colloidosomes, where nanoparticles are wrapped around the oil phase, and Pickering emulsions, where nanoparticles are located at the interface between two liquid phases. [3] The choice of nanoarray structure was motivated by the desire to create a system that could optimize Raman

signal amplification by increasing the density of plasmonic hot spots, [4] thereby improving the electromagnetic enhancement effect. Nanoarrays allow control of the position and spacing between nanoparticles, which is important for the formation of strong and uniform hot spots, which significantly enhances the SERS signal.

Initially, the AgNPs colloid was electrostatically stabilized through TBA^+. Adding ethanol could destabilize the AgNPs colloidal solution and drive them to the water/oil interface. [5] These promoters carry an opposite charge to the nanoparticles and dissolve in the oil layer, reducing interparticle electrostatic repulsion through charge screening. Notably, the promoters do not absorb onto the nanoparticles but instead dissolve in the oil layer. [6] The AgNPs appeared to form island structures on the upper as they moved rapidly to the water/oil interface, an energetically favorable process driven by the reduction in interfacial surface tension. [7] The entire process took less than 20 minutes, during which large-area AgNP arrays gradually formed at the water/air interface, resulting in the fabrication of AgNP films. Then, AgNP nanoarrays were deposited on solid semiconductor wafers based on a previously reported method [8]. The resulting AgNP monolayers appeared white upon reflection, as seen in **Figure S1(a, b, c).** The SEM images (**Figure 9(d, e**)) show that the nanoparticles were arranged regularly next to each other. These interfacial arrays might exhibit significantly enhanced SERS stability compared to simple agglomerated colloids, paving the way for critical SERS studies of surface chemistry.

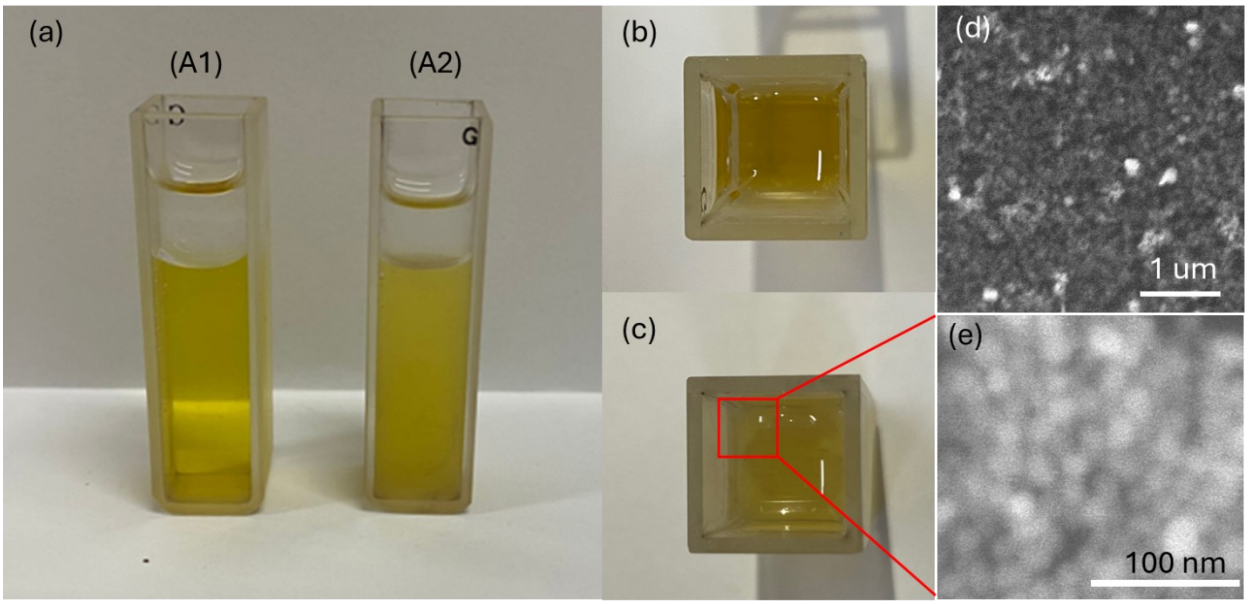

Figure S1. (a) The digital images of (A1) AgNPs colloid/cyclohexane before adding ethanol (A2) AgNPs colloid/cyclohexane after adding ethanol, view from the top of solution (b) before adding ethanol (c) after adding ethanol with the AgNPs layer forming in the interface (d, e) SEM image of silver nanoarray with different magnification.

The results presented in Figure S2 (a, b) demonstrate that substrates prepared with 0.60 mL of hexane in both AgSPA/Cu and AuSPA/Cu exhibited significantly enhanced signals compared to those prepared with 0.45 mL and 0.30 mL of hexane. These findings align well with the Finite Difference Time Domain (FDTD) simulations, which demonstrated that larger AgSPA (or AuSPA) colloidosomes possess good local field enhancement capabilities compared to smaller AgSPA (or AuSPA) colloidosomes, thus confirming the correlation between colloidosome size and SERS signal enhancement. When a high volume of hexane is used in the oil-to-water system, along with an appropriate concentration of $TBANO_3$ and sufficient ultrasonic treatment time, it can lead to the formation of larger AgSPA (or AuSPA) structures. These larger structures enhance the generation of intense hot spots on the colloidosome, which, in turn, increases the Raman signal of the analyte, CV, when it adsorbs onto these nanostructure surfaces.

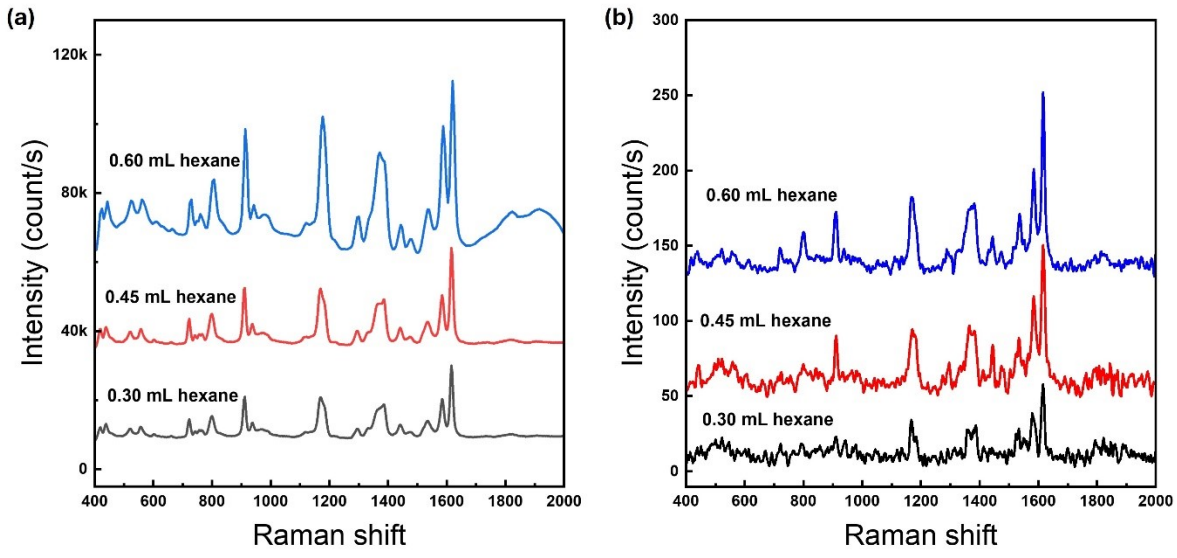

Figure S2. SERS detection of crystal violet (CV) at a concentration of 1.0 ppm, utilizing different substrates: (a) AgSPA/Cu and (b) AuSPA/Cu. These substrates were prepared with varying oil-to-water ratios by adjusting the hexane volumes, which ranged from 0.60 to 0.30 mL.

Limit of detection, limit of quantification, and standard deviation calculation

Standard Deviation of Blank (σ): Measure the response of a blank sample (solvent without analyte) 6 times to determine its standard deviation at peak 911 cm^{-1}

Calculate the Mean (μ) and Standard Deviation (S_D):

- Mean (μ):

$$\mu = \frac{\sum_{i=1}^{n} y_i}{n}$$

where y_i is the intensity of the i^{th} measurement, and n is the total number of measurements.

- Standard Deviation (S_D):

$$S_D = \sqrt{\frac{\sum_{i=1}^{n} (y_i - \mu)^2}{n-2}}$$

Table S1. The signal of a blank sample at 6 times to determine its standard deviation at peak 911 cm^{-1}

Measurement	SERS Intensity (counts)
1	453.8104
2	443.9554
3	463.7414
4	457.5367
5	448.9036
6	450.2243

$$\mu = \frac{\sum_{i=1}^{n} y_i}{n} = \frac{453.8104 + 443.9554 + 463.7414 + 457.5367 + 448.9036}{6} = 453.0286$$

$$S_D = \sqrt{\frac{\sum_{i=1}^{n} (y_i - \mu)^2}{n-2}} = \sqrt{\frac{(453.8104 - 453.0286)^2 + (443.9554 - 453.0286}{6-2}} = 6.969$$

To elaborate on the steps for calculating the Limit of Detection (LOD) and Limit of Quantification (LOQ) in detail

The limit of detection (LOD) was calculated according to the following equation: [9]

$$LOD = 3.3 \times Log\left(\frac{S_D}{b}\right) \text{ (for log(I)=f(logC) linear regression)} \quad (2.1)$$

$$LOD = 3.3 \times S_D/b \text{ (for (I)=f(C) linear regression)} \quad (2.2)$$

The limit of quantification (LOQ) was calculated according to the following equation: [9]

$$LOQ = 10 \times Log(\frac{S_D}{b}) \text{ (for log(I)=f(logC) linear regression)} \quad (2.3)$$

$$LOQ = 10S_D/b \text{ (for (I)=f(C) linear regression)} \quad (2.4)$$

In the case using crystal violet

The linear regression equation was y = (0.30 ± 0.07)x + (3.57 ± 0.19)

X-axis: Logarit the concentration of the analyte.

Y-axis: Logarit of SERS intensity (e.g., the peak intensity at a specific wavenumber, such as 1177 cm^{-1} for CV).

$$LOD = 3.3 \times Log\left(\frac{S_D}{b}\right) = 3.3 \times Log\left(\frac{6.969}{0.3}\right) = 4.51\ ppb$$

$$LOQ = 10 \times Log\left(\frac{S_D}{b}\right) = 10 \times Log\left(\frac{6.969}{0.3}\right) = 13.69 \text{ ppb}$$

In case using thiram

The linear regression equation was y = (224.77 ± 18.91)x + (187.85 ± 269.99)

X-axis: Concentration of the analyte.

Y-axis: SERS intensity (e.g., peak intensity at a specific wavenumber, such as 1386 cm^{-1} for Thiram).

$$LOD = \frac{3.3S_D}{b} = \frac{3.3 \times 6.969}{224.77} = 0.1\ ppm$$

$$LOQ = \frac{10S_D}{b} = \frac{3.3 \times 6.969}{224.77} = 0.3\ ppm$$

The Relative Standard Deviation (RSD) is a statistical measure that expresses the standard deviation

$$RSD\% = \frac{\mu}{S_D} \times 100$$

Table S2. The signal of the sample at 20 times to determine its relative standard deviation at peak 1177, 1588, 1618 cm^{-1}

Measurement	SERS Intensity (counts)		
	1177 cm^{-1}	1588 cm^{-1}	1619 cm^{-1}
1	63846.7	63872.7	63520.7
2	67734.6	58074.0	61078.6
3	69391.9	66144.1	64453.6
4	74107.2	68421.3	68528.1
5	68979.6	58074.0	61078.6

6	71805.8	65680.3	69450.5
7	64673.2	56190.9	60906.8
8	67600.4	55022.7	59996.7
9	66005.6	50890.7	55237.2
10	57391.1	59826.9	62637.7
11	67684.2	60473.3	49991.7
12	55933.7	38933.4	43195.6
13	68979.6	58074.0	61078.6
14	73262.5	64708.4	67393.0
15	69279.6	53868.9	57260.6
16	57223.5	33556.0	42180.6
17	64330.7	46547.8	52134.1
18	58568.8	44547.7	48908.1
19	64900.3	55669.9	47979.8
20	68397.8	54583.7	59673.5

Calculate the Mean (μ) and Standard Deviation (S_D):

- Mean (μ):

$$\mu = \frac{\sum_{i=1}^{n} y_i}{n}$$

where y_i is the intensity of the ith measurement, and n is the total number of measurements.

- Standard Deviation (S_D):

$$S_D = \sqrt{\frac{\sum_{i=1}^{n} (y_i - \mu)^2}{n-2}}$$

RSD%

1177 cm^{-1}	1588 cm^{-1}	1619 cm^{-1}
8.00	7.61	9.35

It indicates the extent of variability in relation to the mean, helping assess the precision and reliability of the method.

Effect of the substrates

Figure S3 highlights that substrates with increased roughness feature a higher concentration of hotspots, likely linked to enhanced SERS intensities. This emphasizes the critical role of preparing surface roughness to strengthen localized electromagnetic fields that amplify signals in SERS applications. The SEM images of the AgSPA/Cu revealed a higher dispersion of colloidosome structures on the Cu foil (Figure S2(a)) compared to the AgSPA/glass slide (Figure S2(b)). This increased dispersion enhances the intensity of the substrate's hotspots and helps maintain the reproducibility of the substrate in trace analysis.

Additionally, Cu foil exhibited good charge transfer capabilities compared to glass slides. This is vital for SERS as it improves the sensitivity and intensity of Raman signals from analyte molecules adsorbed on the substrate. [10] When AgSPAs were deposited on Cu foil, electron redistribution occurred between the Fermi levels of Ag and Cu. [11] This created an electron-deficient state in the Cu foil and an electron-rich state in the AgSPAs. Moreover, Cu foil's higher thermal conductivity, relative to glass slides, lowered the local substrate temperature during laser irradiation. This thermal property enabled efficient heat dissipation, reducing the laser's heating effect and ensuring stable SERS signals. Besides, a decrease in the material’s electrical conductivity significantly reduced the charge transfer-associated chemical enhancement. [12]

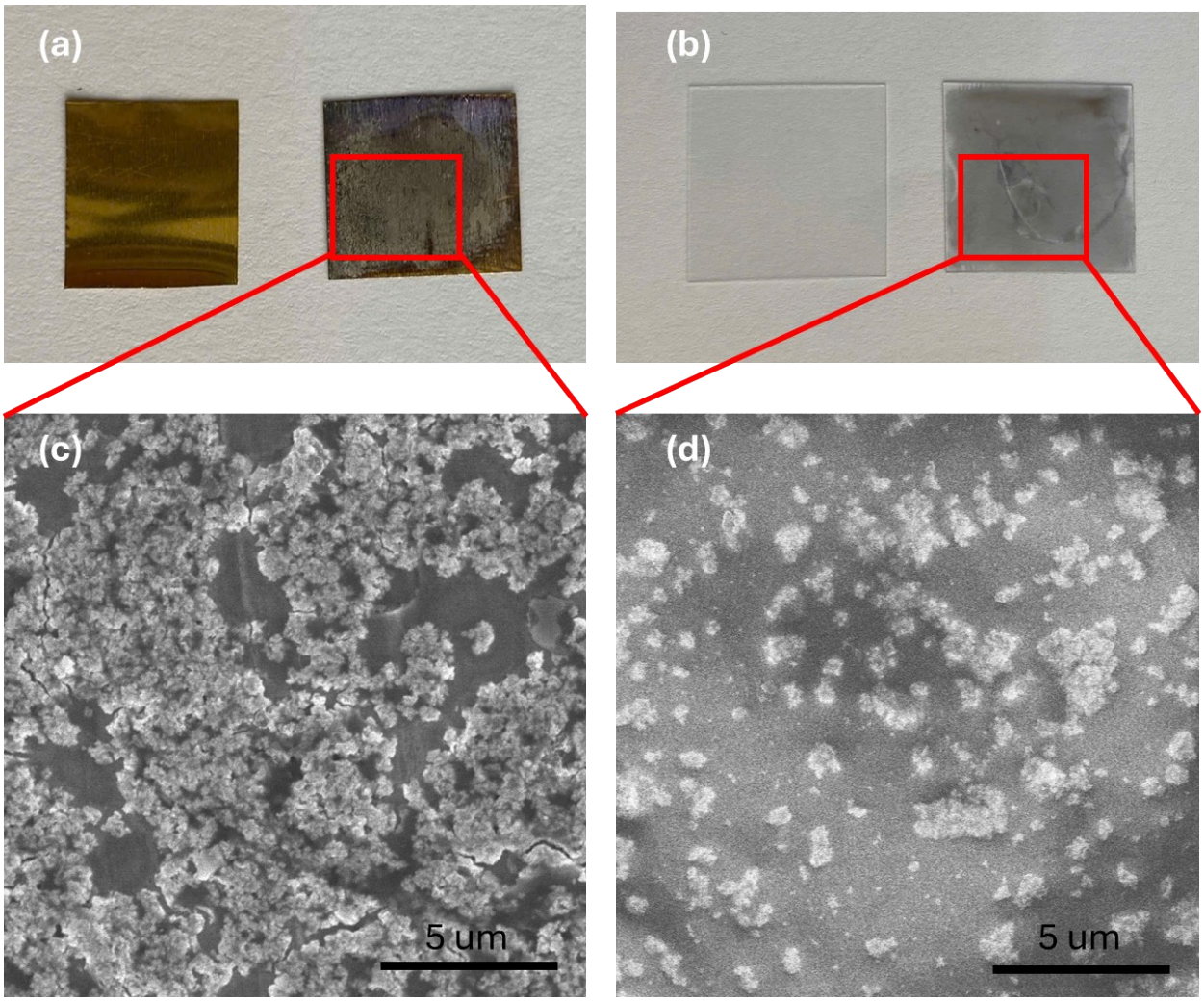

Figure S3. Digital and SEM images of samples were prepared using 0.6 mL hexane for 30 seconds. (a) Digital images: the left shows bare copper foils, and the right shows AgSPA-coated copper foils. (b) Digital images: the left shows a bare glass substrate, and the right shows an AgSPA-coated glass substrate. (c) SEM image of AgSPA/copper foils. (d) SEM image of the AgSPA/glass substrate.

Effect of $TBANO_3$ concentration on SERS performance

The SERS spectra presented in Figure S4 illustrate the detection of Crystal Violet (CV) using Pickering emulsions. The results show that substrates prepared with 1.0 mM TBA^+ exhibited significantly higher SERS signals than those prepared with 5.0 mM TBA^+ and 10.0 mM TBA^+. This observation can be explained by the MWCNT coatings on the outer layer of the emulsions, which were found to reduce the intensity of Ag hot spots, leading to a decrease in the enhancement factor (EF).

Furthermore, Pickering emulsions with higher concentrations of TBA^+, such as 5.0 mM and 10 mM, exhibited lower signal intensities than those with 1.0 mM TBA^+. The increased concentration of promoters led to smaller droplet sizes, affecting the interaction between the laser and the nanostructures. We assume it may be due to the CNT layer at the oil-water interface becoming more tightly packed in emulsions with smaller droplet sizes, reducing the laser's access to the underlying nanostructures. This resulted in lower SERS signal intensity.

Thus, the results suggest that higher concentrations of TBA^+ promote smaller droplet sizes. However, they also limit the laser's ability to interact with the nanostructures due to the compact CNT coating, reducing the SERS enhancement. The 1.0 mM TBA^+ emulsions, with their larger droplet sizes, allow better laser interaction with the nanostructures, resulting in higher signal intensities and better SERS performance.

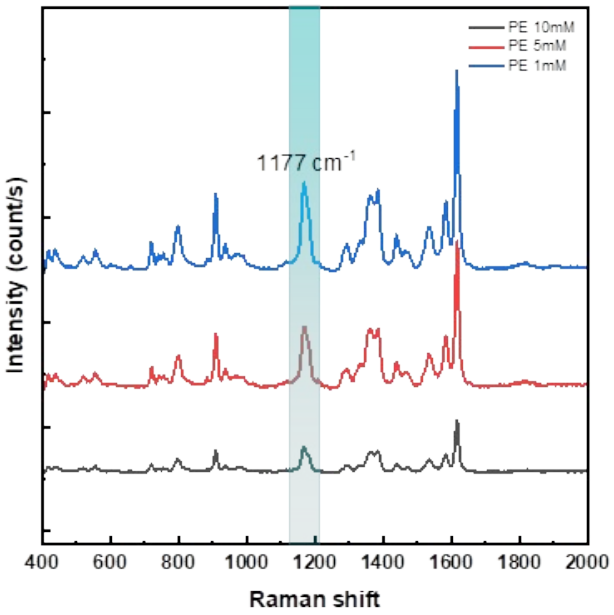

Figure S4. SERS detection of crystal violet (CV) at a 250 ppb concentration using Pickering emulsion substrates prepared with $TBANO_3$ concentrations ranging from 1 mM to 10 mM.

REFERENCES

[1] H.-N. Barad, H. Kwon, M. Alarcón-Correa, and P. Fischer, "Large Area Patterning of Nanoparticles and Nanostructures: Current Status and Future Prospects," *ACS Nano,* vol. 15, no. 4, pp. 5861-5875, 2021/04/27 2021.

[2] X. Zhao, W. Xu, X. Tang, J. Wen, and Y. Wang, "Design of Ag/TiO2/Ag Composite Nano-Array Structure with Adjustable SERS-Activity," vol. 15, no. 20, p. 7311, 2022.

[3] H. Salminen, T. Helgason, B. Kristinsson, K. Kristbergsson, and J. Weiss, "Formation of nanostructured colloidosomes using electrostatic deposition of solid lipid nanoparticles onto an oil droplet interface," *Food Research International,* vol. 79, pp. 11-18, 2016/01/01/ 2016.

[4] P. Dey, "Aiming for Maximized and Reproducible Enhancements in the Obstacle Race of SERS," (in eng), *ACS Meas Sci Au,* vol. 3, no. 6, pp. 434-443, Dec 20 2023.

[5] F. Reincke, S. G. Hickey, W. K. Kegel, and D. Vanmaekelbergh, "Spontaneous assembly of a monolayer of charged gold nanocrystals at the water/oil interface," (in eng), *Angew Chem Int Ed Engl,* vol. 43, no. 4, pp. 458-62, Jan 16 2004.

[6] Z. Ye, C. Li, Q. Chen, Y. Xu, and S. E. J. Bell, "Ultra-Stable Plasmonic Colloidal Aggregates for Accurate and Reproducible Quantitative SE(R)RS in Protein-Rich Biomedia," (in eng), *Angew Chem Int Ed Engl,* vol. 58, no. 52, pp. 19054-19059, Dec 19 2019.

[7] J. Xu *et al.*, "Effect of surfactant headgroups on the oil/water interface: An interfacial tension measurement and simulation study," *Journal of Molecular Structure,* vol. 1052, pp. 50-56, 11/01 2013.

[8] G. Yang, L. Hu, T. D. Keiper, P. Xiong, and D. T. Hallinan, Jr., "Gold Nanoparticle Monolayers with Tunable Optical and Electrical Properties," *Langmuir,* vol. 32, no. 16, pp. 4022-4033, 2016/04/26 2016.

[9] L. Li *et al.*, "Gold Nanoparticle-Based Peroxyoxalate Chemiluminescence System for Highly Sensitive and Rapid Detection of Thiram Pesticides," *ACS Applied Nano Materials,* vol. 4, no. 4, pp. 3932-3939, 2021/04/23 2021.

[10] J. Langer *et al.*, "Present and Future of Surface-Enhanced Raman Scattering," *ACS Nano,* vol. 14, no. 1, pp. 28-117, 2020/01/28 2020.

[11] M. Ahmad *et al.*, "Fabrication of Bimetallic Cu–Ag Nanoparticle-Decorated Poly(cyclotriphosphazene-co-4,4′-sulfonyldiphenol) and Its Enhanced Catalytic Activity for the Reduction of 4-Nitrophenol," *ACS Omega,* vol. 7, no. 8, pp. 7096-7102, 2022/03/01 2022.

[12] W. Liu *et al.*, "Construction of ultra-sensitive surface-enhanced Raman scattering substrates based on 3D graphene oxide aerogels," *Carbon,* vol. 202, pp. 389-397, 2023/01/15/ 2023.